

Nonequilibrium plasmons in optically excited semiconductors

M. Bonitz

Fachbereich Physik, Universität Rostock, Universitätsplatz 3, D-18051 Rostock, Germany

J. F. Lampin, F. X. Camescasse, and A. Alexandrou

*Laboratoire d'Optique Appliquée, Ecole Polytechnique-Ecole Nationale Supérieure de Techniques Avancées,
Unité Mixte de Recherche du Centre National de la Recherche Scientifique No. 7639,*

Centre de l'Yvette, F-91761 Palaiseau Cedex, France

(Received 4 April 2000)

An analysis of the nonequilibrium plasmon spectrum of optically excited semiconductors is presented. It is shown that semiconductors with preexisting carrier populations, due, e.g., to a prepump or doping, may exhibit a rich collective excitation spectrum including additional plasmon modes. If these modes are weakly damped they give rise to an essential acceleration of thermalization processes. It is found that the most favorable conditions for this effect to appear are low temperature and p doping. These theoretical predictions are fully confirmed by results of comprehensive pump-probe experiments on bulk GaAs in the presence of a prepump and in doped samples.

I. INTRODUCTION

Collective excitations in many-particle systems continue to attract the interest of researchers in many fields. In particular, the important role of dynamical screening of the Coulomb interaction and plasmons in the relaxation behavior of semiconductors has been demonstrated in recent years by many theoretical studies, e.g., Refs. 1–4. While the impact of dynamical screening in equilibrium electron-hole plasmas is rather small—it leads to a slight increase of the collision frequencies of energetic carriers, typically of the order of 10–30 % (see, e.g., Ref. 5)—a more pronounced effect can appear in *nonequilibrium* situations due to qualitative changes in the plasmon spectrum. For optical excitation where a femtosecond laser pulse generates nonequilibrium electron and hole distributions in the respective bands, the most prominent feature is the gradual buildup of the plasmon spectrum and of the screening in an initially unscreened carrier ensemble, which has been successfully computed recently by solving the appropriate quantum kinetic equations.^{4,6} Still, the plasmon spectrum remains equilibriumlike, consisting of an optical and an acoustic mode.

With a small modification of the excitation conditions the situation may be changed qualitatively. As we have demonstrated in a recent experiment,³ the *presence of equilibrium carrier populations* at the time of excitation gives rise to additional nonequilibrium plasmon modes, which may lead to a drastically accelerated carrier thermalization confirming earlier model calculations for bulk and low-dimensional semiconductors.^{1,2,7–9} Moreover, these additional plasmon modes may become an interesting source of THz radiation,^{10,11} in particular in 2D and 1D where their spontaneous growth (plasmon instability) has been predicted.^{7,12,13}

As the existence of thermal carriers, e.g., due to doping, is a situation frequently encountered in devices, their effect on the nonequilibrium plasmon spectrum and the thermalization of electron-hole plasmas is of broad interest, for both optics and transport applications. Therefore, in this paper we

present a detailed theoretical and experimental analysis of these phenomena, extending our previous work.³ (a) The aim of our theoretical part (Secs. II and III) is to understand how these phenomena depend on the experimental conditions, such as concentration and temperature of preexcited electrons or holes on one hand and energy and spectral width of the pump pulse, on the other. It turns out that these questions can be answered by a simple stationary analysis of the nonequilibrium dielectric function in the random phase approximation (RPA). We show that the central quantity of interest is the *total velocity distribution* of electrons and holes, which is trivially computed for all experimental situations. The main prediction is that the most favorable conditions for the excitation of nonequilibrium plasmons are p doping and low temperature, which is fully confirmed by our experiments. Furthermore, the effect of thermal carriers is enhanced if the pump acts high in the band and has a small spectral width. (b) We present results of a comprehensive experimental study (Secs. IV and V) of the role of equilibrium holes in p -doped GaAs as well as of the role of a hot or cold thermalized electron-hole plasma injected by a prepump before the arrival of the pump creating the nonequilibrium population. In all cases, the equilibrium carrier density was kept at much lower levels than the nonequilibrium carrier density. We have used an experimental configuration¹⁴ that allows us to follow selectively the evolution of the nonequilibrium *electron* distribution toward thermalization and, therefore, the effect of the equilibrium populations can be assessed unambiguously without any complications coming from the simultaneous measurement of electron and hole dynamics as in the usual experiments. Finally, in Sec. VI we discuss limitations of our theoretical approach and possible extensions and applications.

II. THEORETICAL DESCRIPTION OF PLASMONS IN SEMICONDUCTORS

In this section we briefly recall the derivation of the nonequilibrium RPA dielectric function and of the dynamically

screened Boltzmann collision integral, and their limitations. (Throughout this paper, we will consider situations where phonon scattering is of minor importance and may be neglected.)

A. Dynamical screening effects on carrier scattering

A consistent microscopic description of laser excitation of electron-hole plasmas in semiconductors including scattering, collective excitations, and dynamical screening can be given in the framework of nonequilibrium Green's functions, e.g., Refs. 15 and 16. The starting points are coupled quantum kinetic equations for the carriers and photons (electromagnetic field and plasmons),¹² which are subsequently simplified by applying various approximations. If the transverse field is treated classically (via Maxwell's equations), one arrives at coupled quantum kinetic equations for the carrier distributions f_e, f_h and interband polarization which contain collision integrals I accounting for all relevant scattering and dephasing processes. If, further, correlations between the carriers are weak,¹⁷ the integrals I are of second order in the dynamically screened Coulomb potential $V_s(t_1, t_2)$ and, due to the two-time structure, fully contain the nonequilibrium plasmon dynamics. Thus, the corresponding quantum kinetic equations are well suited to model the excitation and relaxation dynamics, including the excitation-induced formation of the screening cloud^{4,18} in a previously unexcited semiconductor.

In a *preexcited* semiconductor, on the other hand, the screening cloud has had enough time to form (this time is of the order of $2\pi/\omega_{op}$, where ω_{op} is the optical plasma frequency), and the pump pulse gives rise only to modifications of the screening. In this case, it is reasonable to use the adiabatic approximation leading to an instantaneous retarded screened potential $V_s^R(t, \omega)$, which is obtained by Fourier transformation with respect to $t_1 - t_2$, t being the macroscopic time $t = (t_1 + t_2)/2$. As a consequence, the collision integrals in the kinetic equations become the familiar dynamically screened Boltzmann (or Balescu-Lenard or RPA) integrals. For example, the equations for the electrons and holes ($a, b = e, h$) contain integrals of the type

$$I_{ab,k}(t) = \frac{2}{\hbar} \sum_{qk'} \left| \frac{V_q}{\epsilon(q, t, E_{a,k} - E_{a,k-q} + i\delta)} \right|^2 \times \delta(E_{a,k} + E_{b,k'} - E_{a,k-q} - E_{b,k'+q}) \times \{f_{a,k-q} f_{b,k'+q} (1 - f_{a,k}) (1 - f_{b,k'}) - f_{a,k} f_{b,k'} (1 - f_{a,k-q}) (1 - f_{b,k'+q})\} \Big|_t \equiv \Sigma_{ab,k}^<(1 - f_{a,k}) - \Sigma_{ab,k}^> f_{a,k} \quad (2.1)$$

and analogous integrals involving the interband polarization (see, e.g., Ref. 15). In Eq. (2.1), E denotes the single-particle energies, $\delta \rightarrow +0$, and Σ^{\lessgtr} denote the scattering rates.

Obviously, the magnitude of I and, hence, the collision frequency, crucially depend on the absolute value of the screened potential,

$$V_{s,q}^R(t, \omega) = \frac{V_q}{\epsilon^R(q, t, \omega)}, \quad (2.2)$$

where $V_q = 4\pi e^2 / (\epsilon_b q^2)$ is the bare Coulomb potential and $\epsilon^R(q, t, \omega)$ the retarded dielectric function, which contains the full information on the dynamic properties and plasmon spectrum of the nonequilibrium semiconductor. Due to the frequency dependence of the dielectric function the dynamic scattering rates (2.1) may deviate significantly from the static limit where $V_{s,q}^R(t, \omega) \rightarrow V_{s,q}^R(t, 0) = V_q / \epsilon^R(q, t, 0) = 4\pi e^2 / \epsilon_b [q^2 + \kappa(t)^2] \equiv V_q^{st}(t)$, which is the familiar Debye potential with κ being the inverse screening length. According to Eq. (2.1), particularly strong scattering can be expected if $|\epsilon^R(q, \omega)|$ approaches zero which, as we will see below, is related to the existence of plasmons. In situations where the number of plasmons is increased, this effect may be further enhanced. We will show in Sec. III that this is readily achieved in semiconductors with preexcited thermal carriers.

B. Plasmons

It is instructive to rewrite the condition for vanishing absolute value of ϵ as

$$[\text{Re } \epsilon^R(q, \omega)]^2 + [\text{Im } \epsilon^R(q, \omega)]^2 = 0, \quad (2.3)$$

which is the familiar dispersion relation for longitudinal plasmons. Obviously, it requires that simultaneously $\text{Re } \epsilon^R(q, \omega) = \text{Im } \epsilon^R(q, \omega) = 0$. The solutions of this pair of equations are complex functions $\omega \rightarrow \hat{\Omega}_s(q) = \Omega_s(q) + i\Gamma_s(q)$, $s = 1, 2, \dots$, where Ω and Γ have the meaning of plasmon frequency and damping, respectively, and s labels the modes (for details see Ref. 12). If the plasmon damping is weak, $|\Gamma| \ll \Omega$ and $|\text{Im } \epsilon^R(q, \hat{\Omega})| \ll |\text{Re } \epsilon^R(q, \hat{\Omega})|$, we can apply perturbation theory with the result

$$\text{Re } \epsilon[q, \Omega(q)] \Big|_{\Gamma(q)=0} = 0, \quad (2.4)$$

$$\frac{-\text{Im } \epsilon[q, \Omega(q)] \Big|_{\Gamma(q)=0}}{(d/d\omega) \text{Re } \epsilon[q, \omega = \Omega(q)] \Big|_{\Gamma(q)=0}} \approx \Gamma(q). \quad (2.5)$$

This means that the plasmon dispersion is determined from the real part of the dielectric function alone, whereas the imaginary part of ϵ governs the damping of the mode. Analysis of the dielectric function reveals that $\text{Re } \epsilon(q, \omega)$ is positive for $\omega = 0$ and in the limit $\omega \rightarrow \infty$. Therefore, zeros of Eq. (2.4) appear pairwise, where those with positive derivative, $(d/d\omega) \text{Re } \epsilon[q, \omega = \Omega(q)] > 0$, are collective excitations. In an electron-hole plasma in equilibrium, the real part of the dielectric function may have two minima where $\text{Re } \epsilon(q, \omega) < 0$, corresponding to the optical and acoustic plasmon. With increasing temperature, the plasmon damping increases.¹⁹ However, in nonequilibrium, in particular in optically excited semiconductors, there may exist additional minima of $\text{Re } \epsilon(q, \omega)$ which are related to additional acoustic plasmon modes (see, e.g., Refs. 12 and 9).

Thus, according to Eqs. (2.3)–(2.5) we may conclude that $|\epsilon|$ will be close to zero for any weakly damped plasmon mode $\Omega_s(q)$, resulting in enhanced carrier-carrier scattering. With increasing plasmon damping, the scattering rates (2.1) decrease. But even in the limit $\Gamma_s(q) \rightarrow \Omega_s(q)$, when the

mode can no longer be regarded as a well-defined collective excitation, the dynamic scattering rates usually still significantly exceed the static limit.

C. RPA dielectric function

To analyze the plasmon spectrum under optical excitation conditions we need an appropriate approximation for the dielectric function. A consistent treatment of carrier-carrier scattering and dielectric properties, which properly incorporates correlation effects into the dielectric function, is currently actively investigated (cf., e.g., Refs. 20–29). For the situations we are interested in, where the carrier density is high, however, it is justified to neglect correlations in ϵ and to use the familiar random phase approximation

$$\epsilon(q, t, \omega) = 1 - V_q \sum_a \Pi_a(q, t, \omega), \quad (2.6)$$

where Π_a is the Lindhard polarization function, and the sum runs over electrons and holes. For bulk systems with isotropic distributions $f_a(k)$, the imaginary part of the polarization is evaluated as

$$\text{Im } \Pi_a(q, t, \omega) = -\frac{1}{2\pi\hbar^2} \frac{m_a}{q} \int_{k_a^-}^{k_a^+} dk k f_a(k, t), \quad (2.7)$$

where, $k_a^\pm(\omega, q) = (m_a/\hbar^2 q) |\hbar\omega \pm E_a(q)|$, $E_a(q) = \hbar^2 q^2 / (2m_a)$, and the distributions are normalized according to $n_a = (1/\pi^2) \int_0^\infty dk k^2 f_a(k)$. Correspondingly, the real part is given by

$$\text{Re } \Pi_a(q, t, \omega) = \frac{m_a}{4\pi\hbar^2 q} \mathcal{P} \int_0^\infty dk k f_a(k, t) \ln \left| \frac{k_a^- + k}{k_a^- - k} \frac{k_a^+ - k}{k_a^+ + k} \right|, \quad (2.8)$$

where \mathcal{P} denotes that the principal value has to be taken. This is achieved by analytical integration over the logarithmic singularities, which is easily performed for any (continuous) nonequilibrium distribution. Note that the singularities appear at the boundaries of the zero temperature pair continuum, $k = k_a^\pm$. Thus, according to Eq. (2.4), the dispersion $\Omega_s(q)$ of nonequilibrium plasmons is computed from the real part of Eq. (2.6) using Eq. (2.8) with the actual optically generated electron and hole distribution functions. The plasmon damping, on the other hand, is determined by the imaginary part of the nonequilibrium polarization Eq. (2.7).

D. Conditions for weakly damped acoustic plasmons in nonequilibrium e - h plasmas: Total velocity distribution

A plasmon with wave number q_0 and frequency $\Omega_s(q_0)$ will be weakly damped if $\text{Im } \Pi_a(q_0, \Omega(q_0))$ is small for all carrier species simultaneously. Obviously, this will be the case if the electron and hole distributions are small inside the momentum intervals $[k_e^-(\Omega_s(q_0), q_0), k_e^+(\Omega_s(q_0), q_0)]$ and $[k_h^-(\Omega_s(q_0), q_0), k_h^+(\Omega_s(q_0), q_0)]$, respectively. Due to the different masses of electrons and holes these intervals are shifted with respect to each other. Therefore, it is advantageous to transform to velocity space, by substituting $k = m_a v_a / \hbar$, as then all integration intervals are centered around the same velocity ω/q , and only the spread remains

different for different species, $v_a^\pm = \omega/q \pm \hbar q / (2m_a)$. Introducing further the velocity distribution

$$F_a(v) \equiv m_a^2 v f_a(m_a v / \hbar), \quad (2.9)$$

$$n_a = m_a / (\pi^2 \hbar^3) \int_0^\infty dv v F_a(v),$$

and expanding, in Eq. (2.7), F_a around $v = \omega/q$, we obtain

$$\text{Im } \Pi_a(q, \omega) = -\frac{1}{2\pi\hbar^3} \left\{ F_a\left(\frac{\omega}{q}\right) + \frac{1}{4} \frac{\hbar^2 q^2}{m_a^2} \frac{d^2}{dv^2} F_a\left(\frac{\omega}{q}\right) + O(q^4) \right\}. \quad (2.10)$$

Let us analyze the consequences of Eq. (2.10) for plasmons where $q \rightarrow q_0$ and $\omega \rightarrow \Omega(q_0)$, and the central velocity becomes just the phase velocity of the plasmon $v_{ph}^s(q_0) = \Omega_s(q_0)/q_0$. The plasmon damping depends on the sum of the individual polarizations of all components,

$$\text{Im } \Pi[q_0, \Omega_s(q_0)] = -\frac{1}{2\pi\hbar^3} \left\{ F[v_{ph}^s(q_0)] + \frac{\hbar^2 q_0^2}{4} \times \sum_a \frac{1}{m_a^2} \frac{d^2}{dv^2} F_a[v = v_{ph}^s(q_0)] + O(q^4) \right\}, \quad (2.11)$$

with

$$F(v) \equiv \sum_a F_a(v), \quad (2.12)$$

where we introduced the total velocity distribution F . The main contribution arises from the first term in parentheses, which is of the order of the number of particles moving with the phase velocity of the wave. (This is similar to the classical Cerenkov resonance condition.) The second term gives the leading quantum correction, which is important only in the case of collective excitations with large wave number and if the curvature of the individual distributions at the position of the phase velocity is sufficiently large. Finally, we obtain for the imaginary part of the dielectric function that governs the damping [cf. Eqs. (2.6) and (2.11)], keeping only the leading term,

$$\text{Im } \epsilon[q_0, \Omega_s(q_0)] \approx \frac{e^2}{\hbar^3 \epsilon_b} \frac{F[v_{ph}^s(q_0)]}{q_0^2}. \quad (2.13)$$

Now, what about the conditions for the *existence* of acoustic plasmons? In an electron gas in equilibrium, the distribution function $f_e(k)$ is monotonically decreasing, and $F(v)$ is decreasing too, except for the trivial minimum at $v = 0$ [cf. definition (2.9)]. This corresponds to the existence of a single (optical) plasmon. In an equilibrium e - h plasma, $f_e(k)$ and $f_h(k)$ are both monotonically decreasing; how-

ever, in $F(v)$ a minimum appears at finite v between the maxima of $F_h(v)$ and $F_e(v)$. This minimum is around v_{ac}^{eq} —the phase velocity of the familiar equilibrium acoustic plasmon—which is strongly damped due to the large number of electrons and holes moving with $v = v_{ac}^{eq}$ [cf. Eq. (2.13)]. Now, it is easy to imagine that, if *nonequilibrium distributions* $f_e(k), f_h(k)$ are excited that have more than one maximum, the velocity distribution may obtain additional minima. The analysis of Eq. (2.4) then reveals that this may give rise to additional *nonequilibrium acoustic plasmons*. This is most easily understood for the idealized case of distributions with sharp maxima,⁷⁻⁹ $f_a(k) = \sum_{i=1}^{M_a} A_i \Theta(k_{2i}^{(a)} - k) \Theta(k - k_{1i}^{(a)})$, $a = e, h$, which leads to a velocity distribution $F(v)$ with sharp peaks separated by up to $M_e + M_h - 1$ minima. For a mode with phase velocity between the i th peak of F_e and the j th peak of F_h (where $k_{2i}^{(e)} < k_{1j}^{(h)}$), it follows that

$$v_{ph}^{ij} \approx \hbar \frac{k_{2i}^{(e)} + k_{1j}^{(h)}}{m_e + m_h} \quad \text{and} \quad q_{max} \approx 2 \frac{m_e k_{1j}^{(h)} - m_h k_{2i}^{(e)}}{m_e + m_h}. \quad (2.14)$$

Since in this case $F(v_{ph}^{ij}) = 0$, according to Eq. (2.13), this mode is undamped, but it exists only up to a maximum wave number $0 < q_0 < q_{max}$ and only if $q_{max} > 0$. Despite its model character, this example is useful as it gives the upper limit on the number of plasmons, wavelength domain, and degree of undamping. Of course, for realistic nonequilibrium distributions, the damping of the modes is larger [see Eq. (2.10)], and the wave-number range is reduced. Most importantly, however, it turns out that the existence of a plasmon and the value of its phase velocity depend only weakly on the detailed shape of the distribution. They are mainly *determined by the number of peaks of the velocity distribution $F(v)$ and by their location*, and only weakly depend on the shape of the peaks.

Summarizing our analysis, we conclude: (I) there are as many acoustic plasmons possible as the total velocity distribution $F(v) \equiv \sum_a F_a(v)$ has minima (excluding $v = 0$); (II) the damping of a given plasmon with phase velocity $v_{ph} = \Omega/q_0$ is small if $F(v_{ph})$ is small, i.e., if v_{ph} is located in a minimum of F ; (III) the damping depends more sensitively on the heavy component, because $F_a \sim m_a^2$; (IV) the damping is further reduced if the curvature of F (i.e., F'') around v_{ph} is small, i.e., if the corresponding minimum of F is broad.

III. PLASMONS IN SEMICONDUCTORS WITH PREEXISTING CARRIERS

In semiconductors, there exist various possibilities of generating nonequilibrium velocity distributions $F(v)$ with multiple peaks. One is carrier acceleration in an external field; another is optical excitation of nonequilibrium carriers high in the band. Equilibrium electrons and holes are easily generated either by an optical prepump or by using doped samples. Particularly broad opportunities exist in multiband or multisubband systems where energetic carriers can be placed selectively in a chosen subband, thus giving rise to a total distribution with multiple peaks. Nevertheless, only recently was it possible to demonstrate experimentally the effect of nonequilibrium plasmons in pump-probe measurements on bulk GaAs,³ as discussed in Sec. IV. We now apply

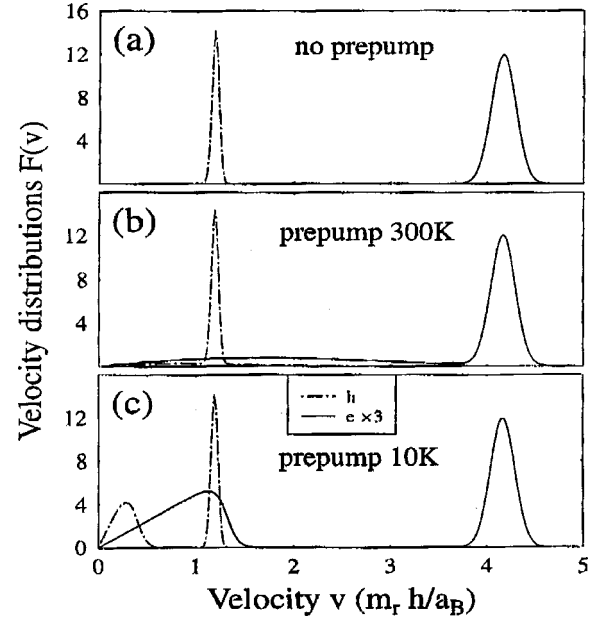


FIG. 1. Electron and hole velocity distribution functions for the case without prepump (top panel) vs with prepump excited equilibrium carriers at 300 K (middle panel) and 10 K (bottom panel). The density of equilibrium and nonequilibrium carriers is $8 \times 10^{16} \text{ cm}^{-3}$ and $3 \times 10^{17} \text{ cm}^{-3}$, respectively. m_r is the reduced mass.

the theoretical results to the situation of these experiments.

We consider bulk GaAs excited by a pump pulse where (A) the material is not preexcited, (B) equilibrium electrons and holes have been generated by a prepump and (C) either equilibrium electrons or equilibrium holes are present—due to n or p doping, respectively. Our main interest is in the influence of the preexisting equilibrium carriers on the electron and hole distribution functions and on the nonequilibrium plasmon spectrum. The distribution functions f_e and f_h are the sum of equilibrium and nonequilibrium components, $f_a(k) = f_a^{eq}(k) + f_a^p(k)$, where the first are Fermi functions of given density and temperature, and for the holes one average (over heavy and light hole bands) population is used. The pump excited nonequilibrium contributions to the two distributions are equal, $f_e^p(k) = f_h^p(k)$, and are modeled as Gaussians centered around the momentum $k = k_0$ according to the laser energy in excess of the band gap. The height and width of the peak are computed from the estimated total carrier density created by the pump and its spectral width, respectively (for the experimental parameters, see Secs. IV and V). Of course, this provides only a rough estimate for the nonequilibrium part of the distributions, as broadening during the rise time of the pulse and due to scattering and dephasing processes is neglected, but this should not affect the comparison of cases (A)–(C). Moreover, the qualitative shape of the distributions—in particular their extrema and peak positions which, as we have seen in the previous section, determine the number and dispersion of plasmons—are reproduced correctly.

A. No preexcited thermal carriers

Figure 1 shows the velocity distributions corresponding to the measurements with and without a prepump. The upper

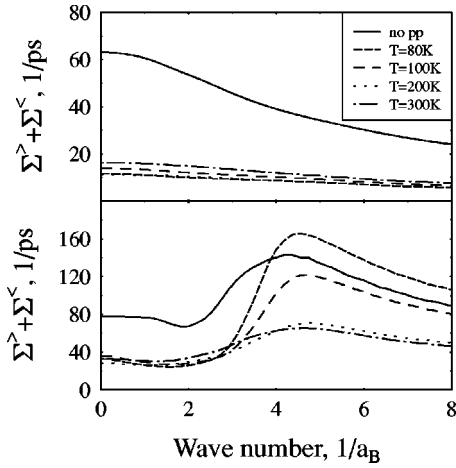


FIG. 2. Static (upper panel) vs dynamic (lower panel) total carrier-carrier scattering rates for varying temperature of the prepump excited equilibrium population. The full line denotes the case without prepump.

figure demonstrates that the pump alone already generates a total distribution $F = F_e + F_h$ with a broad and deep minimum, since, due to the different masses, the maxima of F_e and F_h are displaced with respect to each other. Thus, the existence of one undamped acoustic mode is expected with roughly $v_{ph} \approx 2\hbar k_0 / (m_e + m_h)$ and k_0 denoting the peak of $f(k)$, which is indeed confirmed by the solution of Eqs. (2.4) and (2.5) (cf. the full line in Fig. 4 below).

B. Effect of a prepump

The effect of the prepump carriers (lower two parts of Fig. 1) is twofold. On one hand, these thermal carriers (especially the electrons) “leak” into the minimum of F_v generated by the pump (upper part of Fig. 1) and thus increase the damping of the acoustic mode [cf. Eq. (2.10)]. This effect decreases with decreasing temperature of the prepump carriers and, for the experimental conditions, is negligible below about 100 K. Obviously, increasing the pump energy also reduces this damping effect. A more important second effect is that the thermal carriers (especially the holes) tend to produce a second minimum to the left of the pump excited holes, thus allowing for the excitation of a second acoustic mode. Again, with a reduction of the temperature of the prepump carriers (or with increase of the pump energy), this new minimum becomes deeper, and the damping of the new acoustic mode decreases. As a result, the dynamically screened potential grows at $\omega = \Omega_s$ and $q = q_0$ corresponding to the frequency of the additional plasmon and its wave vector range, leading to increased carrier-carrier scattering. To confirm that this effect is indeed due to plasmons we computed the dynamic and static carrier-carrier scattering rates using the dynamically screened potential (2.2) and the statically screened Coulomb potential V_q^{st} , respectively. Figure 2 shows the result for the case without prepump and for prepump carrier temperatures in the range of 80–300 K. The static rates are insensitive to plasmons and decrease in the presence of a prepump due to the enhanced phase space occupation (Pauli blocking) caused by the preexcited carriers. The dynamic rates, in contrast, show a strong increase with decreasing prepump carrier temperature. At temperatures be-

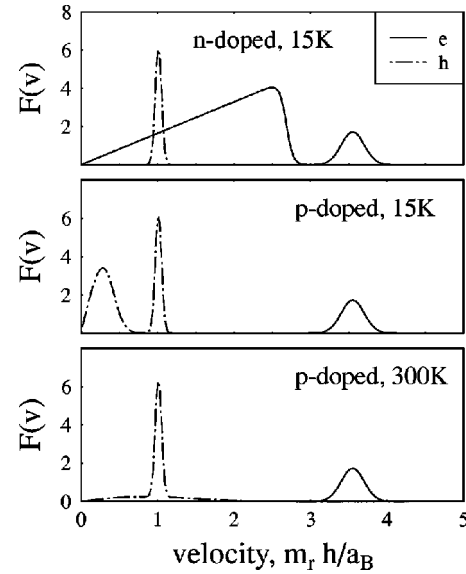


FIG. 3. Electron and hole velocity distribution functions for doped pump excited bulk GaAs. The nonequilibrium carrier density is $1.3 \times 10^{17} \text{ cm}^{-3}$. Top panel: *n*-doped material with equilibrium carriers of temperature 15 K and density $6 \times 10^{17} \text{ cm}^{-3}$. Middle panel: *p*-doped material with equilibrium carriers of temperature 15 K and density $7 \times 10^{16} \text{ cm}^{-3}$. Bottom panel: *p*-doped material with equilibrium carriers of temperature 300 K and density $7 \times 10^{16} \text{ cm}^{-3}$.

low 80 K the rates start to exceed the rates without a prepump. This qualitatively explains the accelerated relaxation observed in the experiments for low prepump carrier temperature (see Sec. V below). A detailed analysis of the experiments shows that accelerated thermalization is observed already at about 200 K (see Fig. 10 below). This difference is readily explained by the broadening of the electron and hole distributions during the rise time of the pump (not accounted for in our model), that leads to an increase of $F(v)$ around $v = v_{min}$ that is independent of the prepump and leads to an increased damping of the first acoustic plasmon. The relative importance of this effect is strongest in the case without prepump, where this plasmon would be undamped otherwise. The plasmon dispersion and damping are similar to those for the case of doping (cf. the next section and Fig. 4 below).

C. Effect of doping

Let us now discuss the effect of preexcited carriers created by *p* or *n* doping. This situation is more easily realized, and it is possible to achieve much lower temperatures of the preexcited carriers. Figure 3 shows the distributions F_e and F_h for the cases of *n* and *p* doping. In both cases, there is a similar tendency to form a second minimum of the total distribution $F(v)$. The top panel shows that *n* doping is not efficient, except for dopant concentrations so small that the corresponding peak of F_e appears well to the left of the pump excited peak of F_h . Clearly, *p* doping (see the lower two panels) is much more favorable for acoustic plasmon undamping than *n* doping. In this case, the low-velocity minimum of $F(v)$ does not interfere with the electron populations. Furthermore, as in the prepump case, reducing the temperature enhances the excitation of plasmons (lower two

panels): the carrier number inside the pump excited minimum of $F(v)$ decreases, and the second minimum at the low-velocity side is becoming more pronounced. Again, the experimental findings and trends are well reproduced.

Finally, Fig. 4 shows the wave-vector dependence of the frequency and damping of the acoustic plasmons calculated from Eqs. (2.4) and (2.5), respectively (the optical plasmon behaves similarly as in equilibrium and is not shown). Clearly, the dispersion of all modes is nearly linear. Further, one sees that, in fact, the dispersion of the first acoustic mode (upper curves in upper panel) changes only weakly in all cases. This confirms our explanation that the dispersion is determined by the (pump-induced) peaks of the electron and hole momentum distribution functions but is insensitive to the further details of their shape. The lower part of Fig. 4 clearly shows that the plasmon damping is strongly decreased if the temperature of the equilibrium carriers is lowered. The additional acoustic mode emerges at low temperatures and exists in a smaller wave-number interval than the first plasmon and is more strongly damped than the latter. At the wave number where the curves end, the damping of the modes becomes comparable to the corresponding plasmon frequency. We mention that the same calculations in the case of n doping yield a second acoustic plasmon only at lower temperature, in a much narrower wave-number range and with a much higher damping than in the case of p doping.

IV. EXPERIMENTAL TECHNIQUE

Pump-probe differential absorption usually reflects the sum of the electron and hole distribution functions. Here we have used a nondegenerate pump-probe scheme that allows us to isolate the electron dynamics: the pump pulse excites electrons from the heavy hole (HH) and light hole (LH) valence bands while the probe pulse measures the absorption saturation of the interband transition from the split-off-hole (SO) valence band to the conduction band C (see Fig. 5). Due to the large spin-orbit splitting in GaAs [340 meV (Ref. 30)] and for not too large pump excess energies with respect to the band gap, no holes are present in the SO band and the differential absorption signal

$$-\Delta\alpha d = -(\alpha_p - \alpha_0)d \quad (4.1)$$

depends on the electron distribution only. α_0 and α_p denote the absorption in the absence and in the presence of the pump, respectively. Since the matrix element of the SO- C transition is isotropic, the measured signal is equally sensitive to the presence of electrons with all possible wave-vector directions. This technique also avoids complications due to coherence effects. The advantages of the nondegenerate pump-probe scheme over the different approaches that have been used to measure carrier relaxation in semiconductors, such as standard pump-probe experiments, time-resolved photoluminescence, and four-wave mixing, have been discussed in more detail in Refs. 32–34.

The samples consist of a GaAs layer ($d=0.65 \mu\text{m}$) sandwiched between two $0.2 \mu\text{m}$ $\text{Ga}_{0.35}\text{Al}_{0.65}\text{As}$ layers grown by molecular-beam epitaxy on a GaAs substrate. The GaAs layer was either undoped or p doped (Be doping). Hall measurements at room temperature yielded $p=5 \times 10^{17} \text{ cm}^{-3}$ for the p -type sample and $p=7 \times 10^{16} \text{ cm}^{-3}$

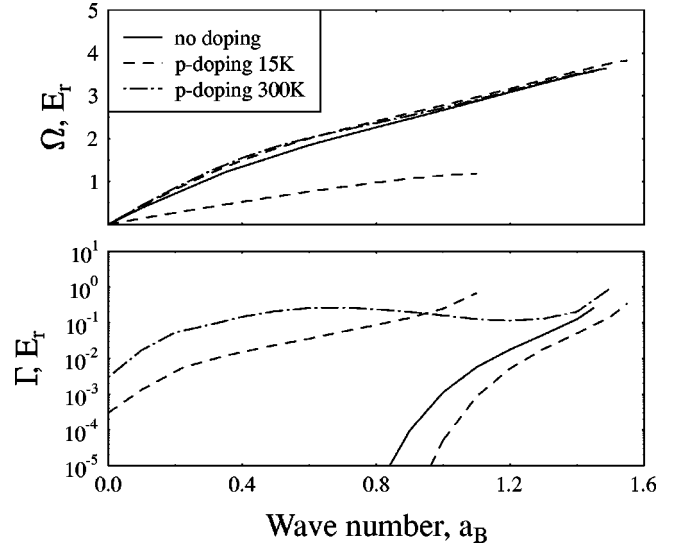


FIG. 4. Dispersion (upper panel) and damping (lower panel) of the acoustic plasmon modes in pump excited bulk GaAs. The curves are for the case without doping (full line) and p -doped material at $T=15 \text{ K}$ (dashes) and $T=300 \text{ K}$ (dash-dotted line). The nonequilibrium carrier density is $1.3 \times 10^{17} \text{ cm}^{-3}$; the equilibrium carrier density of the dopants is $7 \times 10^{16} \text{ cm}^{-3}$.

at 15 K. The substrate was selectively etched away and anti-reflection coatings were deposited on both sides of the sample. Thus, the reflectivity is minimized and the transmitted intensity I_T with and without pump can be directly used to obtain the differential absorption signal:

$$-\Delta\alpha d = \ln(I_{T,\text{with pump}}/I_{T,\text{without pump}}). \quad (4.2)$$

The samples are held either at 15 K on the cold finger of a He compressor cryostat or at room temperature.

The laser setup consists of a Ti:sapphire mode-locked oscillator (Coherent Mira) and a 200 kHz regenerative amplifier system (Coherent RegA) pumped by a single argon-ion laser followed by an optical parametric amplifier (OPA). The regenerative amplifier produces $4 \mu\text{J}$ pulses at 800 nm. $1 \mu\text{J}$ of this output generates a spectral continuum by focusing onto a sapphire crystal. 20% of the continuum is used as the probe pulse. After chirp compensation of the continuum with a combination of prisms and gratings in order to correct up to the third derivative of the phase, we obtain nearly Fourier-transform-limited pulses with a duration of 30 fs for the probe pulse with a practically flat phase in the wavelength range of interest. The rest of the continuum is spectrally filtered using an interference filter and then amplified in a double-stage OPA using two type-I BBO crystals pumped at 400 nm obtained by frequency doubling the remaining $3 \mu\text{J}$ of the regenerative amplifier output. For our three-pulse experiments, we used either a small part of the 800 nm amplified beam as the prepump and the OPA output as the pump (for the low-temperature experiments) or vice versa for the room-temperature experiments. Typical pump and prepump durations were 130–150 fs and the spectral widths were about 15 meV. The beam profiles on the sample were measured using a pinhole. The carrier densities were estimated from the pump excitation density and the measured linear absorption of the sample as well as from the

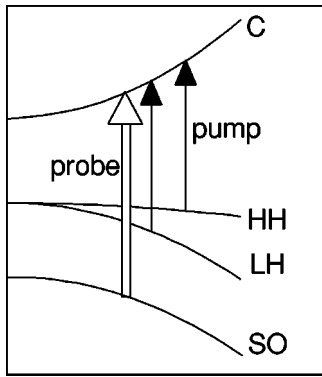


FIG. 5. Schematic of the band structure of GaAs indicating our nondegenerate pump-probe configuration. The transitions undergone under excitation with the pump pulse are shown with single lines and the transitions tested by the probe pulse with double lines.

spectrally integrated differential absorption signal at the end of the pump pulse. The rise time of the spectrally integrated signal as a function of delay time agrees with the pump duration determined from the pump autocorrelation. The zero delay is defined as the coincidence of the pump and probe maxima and is taken at the middle of the integrated-signal rise time.

The transmitted probe beam was dispersed in a 0.25 m spectrometer and detected with a charge-coupled device (CCD) detector. In order to minimize the noise, a shutter was used in the optical path of the pump and the transmitted probe is detected in the presence and in the absence of the pump at an 8 Hz rate. When a prepump was present as well as a pump beam, the shutter was still placed in the optical path of the pump only. The quantity measured in this case was

$$-\Delta\alpha d = -(\alpha_{p,pp} - \alpha_{pp})d, \quad (4.3)$$

where $\alpha_{p,pp}$ is the absorption in the presence of the pump and the prepump and α_{pp} the absorption in the presence of the prepump only. Thus, this experiment monitors the evolution of the pump injected electrons only while the signal due to the prepump injected electrons is subtracted away. It should be noted, however, that this is true only if we assume that the distribution of the prepump injected electrons is not modified by the presence of the pump injected nonequilibrium electrons. In reality, the preexisting electrons are indeed influenced by the nonequilibrium carriers and a signal due to the modification of their distribution appears in the differential absorption spectrum as discussed in the next section.

We also used a different configuration where the shutter was placed on the optical path of the prepump and the pump was blocked. The signal measured in this case was

$$-\Delta\alpha d = -(\alpha_{pp} - \alpha_0)d \quad (4.4)$$

and reflects the electron distribution injected by the prepump only.

V. EXPERIMENTAL RESULTS

We have performed experiments with different types of preexisting carriers: either the carriers are injected by a prepump in which case both electrons and holes are present or

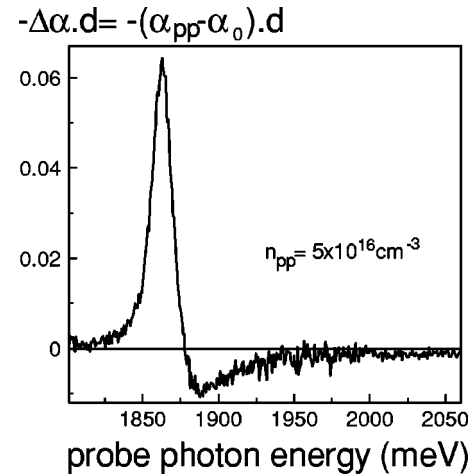


FIG. 6. Differential absorption spectrum in GaAs at 15 K 600 ps after the arrival of the 1.55 eV prepump. The pump was blocked. The prepump injected electron-hole pair density was estimated to be $n_{pp} = 5 \times 10^{16} \text{ cm}^{-3}$.

doping of the material is used and only holes are present. Furthermore, the temperature of the crystal was changed (15 K or 300 K) in order to obtain either cold or hot preinjected carriers. We could thus show the importance of the particular distribution of the preexisting carriers in determining their influence on the relaxation of nonequilibrium electrons.

We will first describe the results obtained in GaAs at 15 K concerning the influence of a cold electron-hole population on the relaxation of nonequilibrium electrons using a prepump of 1.55 eV photon energy arriving on the sample about 600 ps before the pump pulse. The differential absorption spectrum of Fig. 6 reflects the prepump-induced electrons 600 ps after their injection. A comparison with a Fermi-Dirac distribution multiplied by the density of states³⁴ shows that the electron temperature has essentially reached the lattice temperature of 15 K. The negative signal on the high-energy side corresponding to induced absorption can be explained as a modification of the excitonic enhancement.^{14,18,35}

Figure 7, on the other hand, presents differential absorption spectra for different pump-probe delay times showing the pump injected electrons in the presence (a) or in the absence (b),(c) of $5 \times 10^{16} \text{ cm}^{-3}$ cold prepump-induced electron-hole pairs. Two broad peaks at about 1930 and 1970 meV are observed, associated with the nonequilibrium *electron* populations photoexcited from the LH and HH valence bands, respectively. These peaks broaden due to carrier-carrier scattering and evolve toward a thermalized population that can be described by a Fermi-Dirac distribution. At the same time the electrons tend to accumulate at the bottom of the conduction band due to LO-phonon emission. It should be noted that, while the central part of the differential absorption spectrum (1900–2000 meV) indeed reflects the electron distribution, modifications of the excitonic enhancement cause a weak induced absorption at high energies and a modification (shift and broadening) of the SO-C exciton produces the oscillatory structure just below the split-off band gap at 1859 meV.^{14,18,35}

Although the electron-hole pair density injected by the prepump is two times smaller than that injected by the pump,

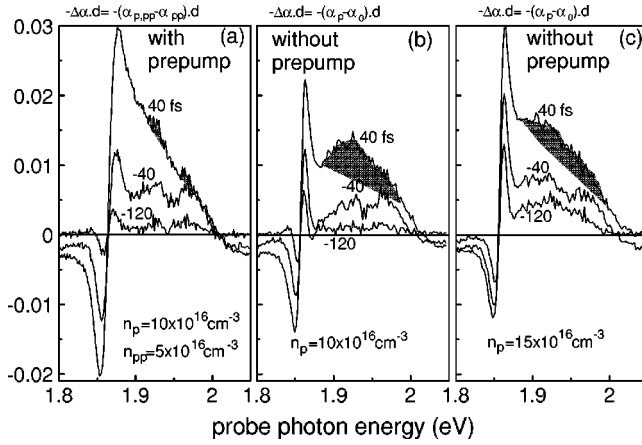


FIG. 7. Differential absorption spectra in GaAs at 15 K in the presence (a) and in the absence [(b) and (c)] of a prepump for a pump energy of 1.607 eV (excess energy with respect to the band gap is 88 meV) for the following pump-probe delay times: -120 , -40 , and 40 fs. (a) The electron-hole pair density injected by the pump (prepump), $n_p(n_{pp})$ was estimated to be $1 \times 10^{17} \text{ cm}^{-3}$ ($5 \times 10^{16} \text{ cm}^{-3}$). (b) $n_p = 1 \times 10^{17} \text{ cm}^{-3}$. The number of electrons “visible” in the differential absorption spectrum is the same as in (a). (c) $n_p = 1.5 \times 10^{17} \text{ cm}^{-3}$, equal to the total density injected by pump and prepump in (a).

it significantly shortens the electron thermalization time, as can be seen by comparing Figs. 7(a) and 7(b). The spectrum shown for a pump-probe delay of 40 fs reflects an electron population that is very close to a thermalized Fermi-Dirac distribution in Fig. 7(a), while a population still far from equilibrium is observed in Fig. 7(b). In order to demonstrate that this difference in thermalization time is not due to the different total carrier densities, we have performed the same experiment as in Fig. 7(b) but with a pump injected carrier density equal to the total density injected by pump and prepump in Fig. 7(a). A comparison of Figs. 7(a) and 7(c) confirms that the presence of the cold carriers injected by the prepump accelerates the relaxation even when the total carrier density is the same. These results are in excellent agreement with the calculations of Sec. III B, which predict an acceleration of the relaxation in the presence of cold prepump-excited carriers due to the formation of a second minimum in the total velocity distribution and to the subsequent excitation of a second acoustic plasmon mode.

Another interesting feature is that in the presence of the prepump [Fig. 7(a)] we observe a more important negative and positive signal around 1850 and 1880 meV, respectively. This is a clear signature of the heating of the cold equilibrium population through Coulomb collisions with the non-equilibrium carriers: cold electrons excited by the prepump occupying states close to the band gap are driven to higher-lying states due to scattering with the non-equilibrium carriers thus leading to an increase in absorption [a larger negative signal than in Figs. 7(b) and 7(c)] around 1850 meV and a decrease in absorption (a larger positive signal) around 1880 meV. The shift to higher energies of the zero crossover point of the spectra in the presence of the prepump confirms the presence of prepump-induced cold electrons occupying the bottom of the conduction band.

The above experiments have shown that cold preinjected electron-hole pairs accelerate the thermalization of nonequi-

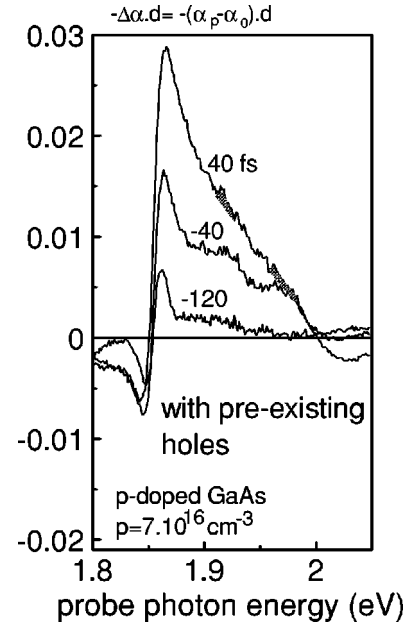


FIG. 8. Differential absorption spectra in *p*-doped GaAs at 15 K for a pump energy of 1.607 eV (88 meV excess energy with respect to the band gap) and for the same delay times as in Fig. 7. The pump-induced carrier density was $1.3 \times 10^{17} \text{ cm}^{-3}$ while the hole density due to the doping was $p = 7 \times 10^{16} \text{ cm}^{-3}$.

librium electrons. In order to determine whether cold electrons or holes are predominantly responsible for this acceleration, we have carried out experiments in *p*-doped GaAs at 15 K where only cold holes are present (Fig. 8) in essentially the same pump excitation conditions (energy and intensity) as in Figs. 7(a) and 7(b). The relaxation of the nonequilibrium electrons in the presence of cold holes is substantially accelerated with respect to the undoped and not preexcited sample [Fig. 7(b)]. In fact, the effect of the cold holes on the relaxation (Fig. 8) is essentially the same as that of cold electron-hole pairs [Fig. 7(a)]. This indicates that equilibrium cold holes are predominantly responsible for the acceleration of the relaxation of nonequilibrium electrons. Also in this case, the conclusion based on the experimental results is in agreement with the theoretical analysis of Sec. III showing that *p* doping, especially at low temperature, is much more favorable than the presence of thermal electrons for the formation of a second minimum in the total velocity distribution and thus for the excitation of a second undamped nonequilibrium acoustic plasmon.

In order to obtain a more quantitative estimate of the acceleration in the different cases, we have compared the differential absorption spectra for a pump-probe delay of 40 fs with those at 200 fs (not shown) where a thermalized electron population that can be described by a Fermi-Dirac distribution with $T = 500$ K has been reached in all cases. We have normalized the areas of the spectra, taken the difference between the spectra at the two delay times, squared, and then spectrally integrated. The result reflects the mean square deviation of the spectral shape at 40 fs from that of a thermalized electron distribution. In the case of preexisting cold holes (Fig. 8) as well as in the case of preexisting cold electron-hole pairs [Fig. 7(a)], the mean square deviation is four times smaller than that in the absence of preexisting

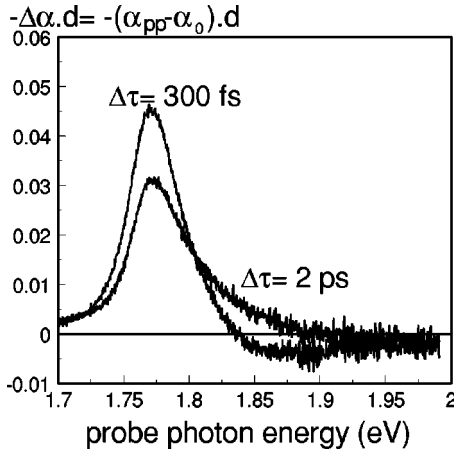


FIG. 9. Differential absorption spectra in undoped GaAs at 300 K for a 1.43 eV prepump (10 meV excess energy with respect to the band gap) for prepump-probe delay times of 300 fs and 2 ps. The pump was blocked. The prepump injected electron-hole pair density was $n_{pp} = 1 \times 10^{17} \text{ cm}^{-3}$.

carriers. This confirms our assertion that cold preexcited carriers accelerate the relaxation and that holes are mainly responsible for this acceleration.

We now turn to the role of the temperature of the preexisting carriers. In order to elucidate its effect, we performed experiments with a low-excess-energy prepump in a room temperature lattice. What happens in this case is that the cold carriers created by the prepump will heat up by phonon absorption and eventually reach the lattice temperature.³⁶ We can thus follow the evolution of nonequilibrium electrons in the presence of *cold* or *hot* preinjected electron-hole pairs, the rest of the experimental conditions being identical. In fact, if the nonequilibrium carriers are injected immediately after the carriers created by the prepump, the latter will still be “cold.” On the other hand, if the nonequilibrium carriers are injected at a later time, the carriers created by the prepump will have reached the lattice temperature (300 K). Figure 9 shows differential absorption spectra reflecting the electrons generated by the prepump only at prepump-probe delay times of 300 fs (after the end of the prepump pulse and before the prepump carriers have reached the lattice temperature) and 2 ps where the electron distribution is a Fermi-Dirac distribution at $T = 300 \text{ K}$. At all delay times after 2 ps, the electron distribution remains identical. Comparing the differential absorption spectrum at 300 fs with a Fermi-Dirac distribution multiplied by the density of states shows that the prepump electrons have already thermalized and have reached a temperature of about 200 K.

After characterizing the electron distribution injected by the prepump, we performed the experiment where both prepump and pump are present in GaAs at 300 K for two different delay times between the pump and prepump maxima: 300 fs and 2 ps. We did not perform experiments for prepump-pump delay times shorter than 300 fs in order to avoid an overlap between pump and prepump. In this way, the density of prepump-excited carriers remains constant during and after the pump pulse. The carrier density photo-created by the prepump and the pump was estimated to be $8 \times 10^{16} \text{ cm}^{-3}$ and $3 \times 10^{17} \text{ cm}^{-3}$, respectively. The differential absorption spectra are shown in Fig. 10 for a pump-

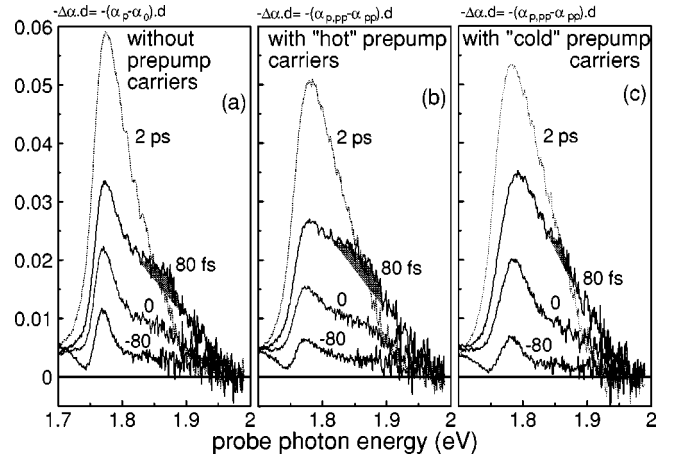


FIG. 10. Differential absorption spectra in undoped GaAs at 300 K in the presence [(b) and (c)] and in the absence of a prepump (a) for a pump energy of 1.544 eV (120 meV excess energy with respect to the band gap) and a prepump energy of 1.43 eV and for the following delay times: $-80, 0, 80 \text{ fs}$, and 2 ps . The prepump- and pump-induced carrier densities were $8 \times 10^{16} \text{ cm}^{-3}$ and $3 \times 10^{17} \text{ cm}^{-3}$, respectively. (b) Pump-prepump delay of 2 ps [the carriers injected by the prepump are “hot” (300 K)]. (c) Pump-prepump delay of 300 fs [the carriers injected by the prepump are “cold” (200 K)].

prepump delay of 2 ps in (b) and of 300 fs in (c) and compared to the spectra in the absence of prepump (a). The two broad peaks observed at low temperature, reflecting nonequilibrium electrons excited from the HH and LH valence bands, are not distinguishable at room temperature; a single broad structure is visible. As was observed in the case of the prepump experiments at 15 K (see Fig. 7), the cold preinjected carriers accelerate the relaxation: whereas in Fig. 10(a), for a pump-probe delay of 80 fs, the peaked structure due to the initially pump injected nonequilibrium electrons around 1.87 eV is still visible, in Fig. 10(c) the nonequilibrium electrons have almost completely redistributed. Nevertheless, when the preinjected carriers are hot [Fig. 10(b)], no such acceleration is observed. On the contrary, the relaxation is somewhat slowed down. This is visible from the fact that the structure due to the nonequilibrium carriers is more prominent for the same delay time of 80 fs. It is confirmed by the calculation of the mean square deviation (as explained above) of the spectral shape at 80 fs from the thermalized one at 2 ps: In the case of cold preexisting electron-hole pairs [Fig. 10(c)], the mean square deviation is 27% smaller than that in the absence of a prepump (a), whereas it is 5% larger in the presence of hot preexisting carriers (b). We have thus demonstrated that the precise distribution function of the preinjected carriers is of fundamental importance in determining their influence on the relaxation of nonequilibrium populations, in agreement with the theoretical predictions of Sec. III B (Fig. 2). Indeed, as explained in Sec. III, an increasing temperature of the preinjected carriers leads to increased damping of the additional acoustic plasmon mode and of the related enhancement of the dynamically screened Coulomb potential. The relaxation of the nonequilibrium electrons is quite different in the presence of hot (300 K) or cold (200 K) pre-injected carriers [cf. Figs. 10(b) and 10(c)]. Probably the difference would be much more pronounced if the same ex-

periment could be performed with lower prepump carrier temperatures but, as mentioned above, this was not possible without the prepump and pump overlapping temporally. It should be noted that the temperature of 200 K cited above corresponds to an average electron temperature (i.e., the prepump carrier temperature experienced by the rising front of the pump is lower while that seen by the trailing edge is higher).

VI. CONCLUSIONS

We have presented a detailed theoretical and experimental analysis of the effect of pre-existing thermal carriers on the relaxation rates of pump-excited carriers in bulk GaAs. We have shown that the equilibrium carriers may have an essential effect at low temperatures due to the excitation of additional weakly damped acoustic plasmons. This leads to strongly enhanced Coulomb scattering, which explains the experimentally observed accelerated thermalization.

While for our experimental situations phonon scattering was negligible, it will be more important at lower densities. In this case, we expect a smaller relative effect of preexcited carriers. Our theoretical analysis can directly be extended to this situation by considering the nonequilibrium spectrum of coupled plasmon-phonon modes.

Our treatment of dynamical screening well explains the general trend of the effect of preexcited carriers. As was discussed above, this is related to the fact that the nonequi-

librium plasmon spectrum is mainly determined by the peaks of the electron-hole velocity distribution, the location of which is only weakly changing during the action of the pump. On the other hand, to obtain quantitative agreement with the measurements, of course a time-dependent theory has to be used. This requires us to solve the semiconductor Bloch equations over a long time that includes the pump and the prepump. Moreover, to correctly describe the plasmon and screening buildup effects, it is necessary to use a full two-time potential.

As can be seen, e.g., from Eq. (2.13) the plasmon damping is always positive. This is a peculiarity of isotropic three-dimensional (3D) systems.³⁷ In contrast, in nonequilibrium 2D and 1D systems, $\text{Im } \epsilon$ may change its sign, resulting in acoustic plasmons of increasing amplitude, i.e., instabilities.^{7,13} Although this has not been observed yet, optical excitation of the necessary nonequilibrium distributions seems possible. A similar role of preexcited carriers is expected for transport measurements.

ACKNOWLEDGMENTS

We are grateful to V. Thierry-Mieg and R. Paniel for the high-quality GaAs samples. We also thank J.-P. Likforman and G. Rey for help with the optical parametric amplifier. M.B. acknowledges support from the DFG (Schwerpunkt ‘‘Quantenkohärenz in Halbleitern’’).

-
- ¹D. C. Scott, R. Binder, and S. W. Koch, *Phys. Rev. Lett.* **69**, 347 (1992).
- ²R. Binder, D. C. Scott, A. E. Paul, M. Lindberg, K. Henneberger, and S. W. Koch, *Phys. Rev. B* **45**, 1107 (1992).
- ³J.-F. Lampin, F.-X. Camescasse, A. Alexandrou, and M. Bonitz, *Phys. Rev. B* **60**, R8453 (1999).
- ⁴L. Bányai, Q. T. Vu, B. Mieck, and H. Haug, *Phys. Rev. Lett.* **81**, 882 (1998).
- ⁵D. O. Gericke, S. Kosse, M. Schlages, and M. Bonitz, *Phys. Rev. B* **59**, 10 639 (1999).
- ⁶H. Haug, in *Progress in Nonequilibrium Green's Functions*, edited by M. Bonitz (World Scientific, Singapore, 2000), pp. 212–225.
- ⁷M. Bonitz, R. Binder, and S. W. Koch, *Phys. Rev. Lett.* **70**, 3788 (1993).
- ⁸K. ElSayed, R. Binder, D. C. Scott, and S. W. Koch, *Phys. Rev. B* **47**, 10 210 (1993).
- ⁹D. C. Scott, R. Binder, M. Bonitz, and S. W. Koch, *Phys. Rev. B* **49**, 2174 (1994).
- ¹⁰R. Kersting, K. Unterrainer, G. Strasser, H. F. Kauffmann, and E. Gornik, *Phys. Rev. Lett.* **79**, 3038 (1997).
- ¹¹R. Kersting, J. N. Heymann, G. Strasser, and K. Unterrainer, *Phys. Rev. B* **58**, 4553 (1998).
- ¹²M. Bonitz, *Quantum Kinetic Theory* (Teubner, Stuttgart, 1998).
- ¹³In this context it is interesting to note similar concepts of exciting plasmon instabilities using an electrical current to generate the nonequilibrium carrier distributions. See, e.g., P. Hawrylak and J. J. Quinn, *Appl. Phys. Lett.* **49**, 280 (1986); P. Bakshi, J. Cen, and K. Kempa, *Solid State Commun.* **76**, 835 (1990); K. Kempa, P. Bakshi, and H. Xie, *Phys. Rev. B* **47**, 4532 (1993), and references therein.
- ¹⁴F. X. Camescasse, A. Alexandrou, D. Hulin, L. Bányai, D. B. Tran Thoai, and H. Haug, *Phys. Rev. Lett.* **77**, 5429 (1996).
- ¹⁵H. Haug and A. P. Jauho, *Quantum Kinetics for Transport and Optics in Semiconductors* (Springer, Berlin, 1996).
- ¹⁶*Progress in Nonequilibrium Green's Functions* (Ref. 6).
- ¹⁷For the treatment of strong correlations which are of importance, e.g., at low temperatures, see Ref. 5.
- ¹⁸Q. T. Vu, L. Bányai, H. Haug, F. X. Camescasse, J.-P. Likforman, and A. Alexandrou, *Phys. Rev. B* **59**, 2760 (1999).
- ¹⁹Notice that, with increasing temperature, the minima of $\text{Re } \epsilon$ move above the ω axis, and Eq. (2.4) would predict that the plasmons vanish. However, in this case the small-damping approximation breaks down and Eq. (2.4) is no longer justified. In fact, the solution of the complex dispersion relation still yields strongly damped plasmons (Refs. 31 and 12).
- ²⁰N. H. Kwong and M. Bonitz, *Phys. Rev. Lett.* **84**, 1768 (2000).
- ²¹W. H. Knox, D. S. Chemla, G. Livescu, J. E. Cunningham, and J. E. Henry, *Phys. Rev. Lett.* **61**, 1290 (1988).
- ²²L. H. Acioli, M. Ulman, F. Vallée, and J. G. Fujimoto, *Appl. Phys. Lett.* **63**, 666 (1993).
- ²³U. Hohenester, P. Supancic, P. Kocevar, X. Q. Zhou, W. Kütt, and H. Kurz, *Phys. Rev. B* **47**, 13 233 (1993).
- ²⁴J. A. Kash, *Phys. Rev. B* **51**, 4680 (1995).
- ²⁵K. El Sayed, S. Schuster, H. Haug, F. Herzel, and K. Henneberger, *Phys. Rev. B* **49**, 7337 (1994).
- ²⁶K. El Sayed, L. Bányai, and H. Haug, *Phys. Rev. B* **50**, 1541 (1994).

- ²⁷W. Schäfer, J. Opt. Soc. Am. B **13**, 1291 (1996).
- ²⁸M. Bonitz, D. Kremp, D. C. Scott, R. Binder, W. D. Kraeft, and H. S. Köhler, J. Phys.: Condens. Matter **8**, 6057 (1996).
- ²⁹R. Binder, H. S. Köhler, M. Bonitz, and N. Kwong, Phys. Rev. B **55**, 5110 (1997).
- ³⁰*Numerical Data and Functional Relationships in Science and Technology*, edited by O. Madelung, Landolt-Börnstein New Series, Group III, Vol. 17, Pt. a (Springer, Berlin, 1982).
- ³¹M. Bonitz, R. Binder, D. C. Scott, S. W. Koch, and D. Kremp, Phys. Rev. E **49**, 5535 (1994).
- ³²F. X. Camescasse, A. Alexandrou, and D. Hulin, Phys. Status Solidi B **204**, 293 (1997).
- ³³A. Alexandrou, V. Berger, and D. Hulin, Phys. Rev. B **52**, 4654 (1995).
- ³⁴A. Alexandrou, V. Berger, D. Hulin, and V. Thierry-Mieg, Phys. Status Solidi B **188**, 335 (1995).
- ³⁵K. El Sayed and C. J. Stanton, Phys. Rev. B **55**, 9671 (1997).
- ³⁶J.-F. Lampin, F. X. Camescasse, V. Thierry-Mieg, and A. Alexandrou, in *Ultrafast Phenomena XI*, edited by W. Zinth, J. G. Fujimoto, T. Elsaesser, and D. Wiersma (Springer, Berlin, 1998).
- ³⁷M. Bonitz, Phys. Plasmas **1**, 832 (1994).